

## Direct discerning reaction pathways in methanol-to-hydrocarbons by transient operation – FASPA

Liu, Chuncheng; Uslamin, Evgeny A.; Pidko, Evgeny A.; Kapteijn, Freek

**DOI**

[10.1016/j.cej.2022.139696](https://doi.org/10.1016/j.cej.2022.139696)

**Publication date**

2023

**Document Version**

Final published version

**Published in**

Chemical Engineering Journal

**Citation (APA)**

Liu, C., Uslamin, E. A., Pidko, E. A., & Kapteijn, F. (2023). Direct discerning reaction pathways in methanol-to-hydrocarbons by transient operation – FASPA. *Chemical Engineering Journal*, 453, Article 139696. <https://doi.org/10.1016/j.cej.2022.139696>

**Important note**

To cite this publication, please use the final published version (if applicable). Please check the document version above.

**Copyright**

Other than for strictly personal use, it is not permitted to download, forward or distribute the text or part of it, without the consent of the author(s) and/or copyright holder(s), unless the work is under an open content license such as Creative Commons.

**Takedown policy**

Please contact us and provide details if you believe this document breaches copyrights. We will remove access to the work immediately and investigate your claim.



# Direct discerning reaction pathways in methanol-to-hydrocarbons by transient operation – FASPA

Chuncheng Liu<sup>a,b</sup>, Evgeny A. Uslamin<sup>b</sup>, Evgeny A. Pidko<sup>b,\*</sup>, Freek Kapteijn<sup>a,\*</sup>

<sup>a</sup> Catalysis Engineering, Department of Chemical Engineering, Delft University of Technology, Van der Maasweg 9, 2629 HZ Delft, the Netherlands

<sup>b</sup> Inorganic Systems Engineering, Department of Chemical Engineering, Delft University of Technology, Van der Maasweg 9, 2629 HZ Delft, the Netherlands

## ARTICLE INFO

### Keywords:

Transient operation  
Stimulus-response analysis  
FASt Scanning-Pulse Analysis  
Methanol-to-hydrocarbons  
Aromatization

## ABSTRACT

Monitoring complex catalytic pathways under industrially-relevant conditions is one of the key challenges in catalysis chemistry and technology. Herewith we describe a direct technique called ‘fast scanning-pulse analysis’ (FASPA) that allows the direct characterization and detailed kinetic analysis of intimately interweaved catalytic pathways. The power and potential of the FASPA approach are demonstrated with an industrially relevant methanol-to-hydrocarbons (MTH) process over H-ZSM-5 zeolite. This reaction proceeds via a hydrocarbon pool (HCP) mechanism producing olefins and aromatics. The HCP is built-up upon exposure to methanol during the induction period, followed by a transition regime to a *quasi* steady-state MTH operation. This FASPA technique allows (sub-)second resolution of the full temporal products response upon a methanol pulse providing direct and quantitative insights into the MTH reactions. Globally, two consecutive pathways can be discerned: a very fast primary product formation in the presence of methanol in a narrow active MTH reaction zone, followed by a slower formation of light aromatics, which is closely related to the decomposition and release of HCP species and secondary reactions in absence of methanol in the downstream part of the catalyst bed. The time delay between the appearance of inert tracer and primary products represents the time needed to build-up the HCP in the induction period, where methane is observed prior to other products. The primary products (alkanes, olefins, and light aromatics) are nearly instantaneously formed from the pulsed methanol. These results demonstrate the highly dynamic character of the HCP in the MTH process over H-ZSM-5.

## 1. Introduction

Elucidating the reaction mechanism and kinetics analysis is essential for rational catalyst design and process optimization. However, the direct characterization of multistep reaction networks under operating conditions remains challenging because of the strong interplay between the substrates involved in different elementary steps. Moreover, limiting tools to determine the product distribution in a transient study of a complex reaction network hinders the direct monitoring of the reaction mechanism and the quantitative analysis to harvest the full kinetic information. The hydrocarbon conversion such as methanol-to-hydrocarbons (MTH) in the zeolite-type catalysts represents a prominent case of a catalytic process facing these complexities. The synthesis of hydrocarbons from the MTH process presents an alternative way to reduce fossil fuel reliance, while methanol (MeOH) can be generated from various substrates such as CO<sub>2</sub>, natural gas, and biomass [1–5]. In particular, the production of biomethanol from municipal solid waste is

a promising solution for regions such as Europe when searching for alternative routes and low-cost fossil-based feedstocks for the production of biofuels [6]. The thermochemical process for biomethanol production involves the gasification of waste feedstock to generate syngas (*i.e.* CO<sub>2</sub>, CO and hydrogen) and its subsequent catalytic synthesis [7], although harsh reaction conditions such as high temperature and low conversion efficiency hinder the wider application of biomethanol production at full scale [8,9].

Even though the MTH reaction mechanism has been studied extensively for > 40 years, there are still ongoing debates over two key aspects: 1) the initial direct C–C bond formation and 2) the reaction pathways for the formation of various hydrocarbons and their connection to intra-zeolite ‘hydrocarbon pool’ (HCP) species. The lack of versatile experimental research methods, which must be space- and time-resolved and applicable under actual reactive conditions, adds to the challenge to investigate such a complex system. Although the recent advent of sophisticated characterization technologies such as *in situ*

\* Corresponding authors.

E-mail addresses: [e.a.pidko@tudelft.nl](mailto:e.a.pidko@tudelft.nl) (E.A. Pidko), [F.Kapteijn@tudelft.nl](mailto:F.Kapteijn@tudelft.nl) (F. Kapteijn).

<https://doi.org/10.1016/j.cej.2022.139696>

Received 22 July 2022; Received in revised form 4 October 2022; Accepted 5 October 2022

Available online 8 October 2022

1385-8947/© 2022 The Authors. Published by Elsevier B.V. This is an open access article under the CC BY license (<http://creativecommons.org/licenses/by/4.0/>).

solid-state NMR provided more solid experimental evidence and further insights explaining the initial direct C–C bond formation, [10–13] solid experimental evidence obtained under real experimental MTH conditions (e.g., > 400 °C) is still very limited. Note that olefins and other products are generated almost immediately after a relatively short induction period after the initial C–C formation, especially at industrial temperature levels, resulting in the so-called *quasi* steady-state operation [14]. A HCP mechanism was proposed especially in CHA-type zeolites (such as H-SAPO-34 and H-SSZ-13) with a cage-window structure (in contrast with the channel-intersection structure of MFI-type H-ZSM-5) to explain the final hydrocarbon formation [15]. Based on this concept, formed hydrocarbon intermediates (preferably described as cyclic or aromatic compounds) are trapped in the cage. The final products such as light olefins are split-off products from these active pool species. Studying these reaction routes of MTH and the accompanying kinetic research under industrially-relevant conditions are challenging due to the extremely fast methanol conversion rate (autocatalytic process), where many closely related elementary steps occur nearly instantaneously [16]. In fixed bed operation generally full MeOH conversion is obtained, implying a small reaction zone that gradually moves through the catalyst bed during the slow catalyst deactivation [17,18].

So far, several transient kinetic techniques such as the temporal analysis of products (TAP) and  $^{12}\text{C}/^{13}\text{C}$  isotope labelling have been utilized to obtain highly specific mechanistic and kinetic information, especially on the MTH mechanism [19,20]. However, the challenging transient data analysis heavily relying on mass spectrometry in the TAP setup [21] limits the discrimination of specific individual reaction steps such as olefin methylation or cracking in the MTH [20,22], since they can affect each other in such a complex reaction network. Detailed mechanistic and kinetic information can be extracted from  $^{12}\text{C}/^{13}\text{C}$  labelling experiments, but the off-line GC–MS (Gas Chromatography–Mass Spectrometry) analysis implies that a continuous and instant temporal product distribution is not accessible. Pulse-quench methods combined with spectroscopic measurements are also used to investigate the transition from the induction period to the steady-state formation of hydrocarbons on a running zeolite catalyst [23,24]. *Ex-situ*  $^{13}\text{C}$  CP/MAS NMR (Cross-Polarization Magic-Angle-Spinning Nuclear Magnetic Resonance) spectroscopy measurements on the quenched zeolite catalysts after the ethylene pulse revealed that 1,3-dimethylcyclopentenyl carbenium ions were produced almost instantaneously above 350 °C. At elevated temperatures, the presence of such species on a working zeolite catalyst greatly decreases the induction duration and speeds up the methylation rate in the ethylene-to-toluene process, suggesting active participation of these species in the HCP [23,24]. More intriguingly, if the time interval between ethylene pulses is long, the kinetic induction phase is resumed, indicating the reactive and dynamic nature of these HCP species. However, owing to the rapid generation and degradation (in seconds) of these entrapped species, including methylcyclopentadienes and methylbenzenes via, respectively, deprotonation and ring expansion of 1,3-dimethylcyclopentenyl ions [24], the online measurement of gaseous hydrocarbon products is difficult, especially on the working catalyst.

In this work, a newly developed transient kinetics technique is introduced, based on a combination of stimulus–response operation with fast scanning-pulse analysis by GC, coined FASPA, and *in situ* DRIFT spectroscopy measurement. The combination of repetitive MeOH pulse injections and fine control of the online GC sampling delay allows a quantitative mapping of the fast temporal evolution of the products responses upon a MeOH pulse, even when the GC analysis is far slower. Based on the moment analysis of transient products responses, kinetic information on their formation in the MTH process can be further extracted. After a careful validation of this approach, the dynamic features of the MTH process over H–ZSM-5, including direct MeOH transformation, secondary reactions, and decomposition/desorption processes, are decoupled and analysed quantitatively. Combining pulse and *in situ* DRIFT experiments, the fast instantaneous formation of

aliphatic species and aromatics is attributed to the induction-transition period for HCP build-up, whereas a following second aromatics formation is a result of desorption/decomposition of HCP species and secondary reactions in the downstream region of the bed.

## 2. Material and methods

### 2.1. Zeolite samples and chemicals

ZSM-5 (NH<sub>4</sub>-ZSM-5, Si/Al 25) and silicalite-1 were received from BASF. After calcination in air at 550 °C (2 °C/min) for 6 h, the obtained zeolites are further denoted as H-ZSM-5 (protonic form) and Sil-1, respectively. The calcined zeolite powder was compressed, crushed, and sieved to a particle size fraction of 150–212 μm.

All reagents were of reagent grade and used without further purifications: methanol (MeOH, Sigma-Aldrich, for HPLC, ≥ 99.9 %), dimethyl ether (DME, 25 vol% in Ar), propylene (8 vol% in He), and deionized water.

### 2.2. Catalyst characterizations

Zeolite morphology was determined by carrying out scanning electron microscopy (SEM) imaging using a JEOL JSM-6010LA with a standard beam potential of 10 kV and an Everhart-Thornley detector.

X-ray powder diffraction (XRD) was performed in Bragg-Brentano geometry with a Bruker D8 Advance X-ray diffractometer using monochromatic Co Kα ( $\lambda = 1.788970 \text{ \AA}$ ) radiation between  $2\theta = 5^\circ$  and  $55^\circ$ . Microporous properties of H-ZSM-5 sample were assessed from N<sub>2</sub> physisorption isotherms at -196 °C using Tristar II 3020. Prior to the measurements, the sample was dried and degassed at 350 °C for 6 h under constant N<sub>2</sub> flow.

Transmission FT-IR (Fourier Transform infrared) spectroscopy of adsorbed pyridine as a probe molecule was used to quantify the acid site density. H-ZSM-5 sample (~25 mg) was pressed in a self-supported wafer with a diameter of 1.6 cm and then placed in an IR quartz cell. The spectra were collected at 2 cm<sup>-1</sup> resolution using a Nicolet Nexus spectrometer equipped with an extended KBr beam splitting and an MCT detector. The concentration of Brønsted acid sites (BAS) and Lewis acid sites (LAS) was derived from the absorbance at 1545 and 1456 cm<sup>-1</sup> using the integrated molar extinction coefficients of 0.73 and 1.11, respectively. [25] Assuming that one pyridine molecule is only adsorbed on one BAS/LAS, the following equations were used to estimate C<sub>BAS</sub> and C<sub>LAS</sub>:

$$C_{\text{BAS}} = 4.30 \times IA(\text{BAS})R^2/W \quad (1)$$

$$C_{\text{LAS}} = 2.83 \times IA(\text{LAS})R^2/W \quad (2)$$

where *IA* (BAS, LAS) represents the integrated absorbance of the band at 1545 and 1456 cm<sup>-1</sup>, *R* is the radius of a sample wafer (cm) and *W* is the weight of a sample wafer (g).

### 2.3. Catalytic testing

Three types of experiments were carried out with freshly activated catalyst samples:

- FASPA experiments with MeOH over different catalyst loadings, reaction temperatures, MeOH injected amounts and MS analysis
- FASPA experiments with propylene
- Pulse series experiments with *in situ* DRIFT measurements using dimethyl ether

Pulse tests and MTH continuous performance tests were carried out at 390–420 °C using a fixed-bed reactor setup. A 4 mm (ID) quartz tube reactor was filled with catalyst amounts of 4.5, 50, 100 or 200 mg sieved

zeolite fraction (particle size 150–212  $\mu\text{m}$ ). Samples below 100 mg were diluted with SiC to a bed volume equivalent to 100 mg catalyst. The catalyst was activated at 550  $^{\circ}\text{C}$  with 10 mL/min air for 1 h before cooling down to the reaction temperature. After passing through the thermostatic saturator with liquid MeOH, a mixture of MeOH/Ar/He (Ar used as internal standard) was fed into the sample loop of the six-port valve equipped with a universal actuator (VICI VALCO, USA). The reactant mixture was pulsed to the reactor using 20 mL<sub>NTP</sub>/min He as a carrier gas. The products were analyzed by an online MS (Pfeiffer, ThermoStar GSD320-QMG220) and a Thermo Trace GC. The reaction products ranging from methane to trimethylbenzene (TriMB) with only traces of tetramethylbenzene (TetraMB) were observed.

### 2.3.1. Fast scanning-pulse GC test protocol

The conventional GC analysis of the MTH product mixture takes too long to obtain a real-time quantitative mapping of the temporal product spectrum upon a MeOH pulse injection. An option is to sample the product response to a MeOH pulse over the MTH catalyst by a multi-position sampling valve and analysis off-line [23,24], which obviously yields a lower density of data points during the transient operation. In our study we have chosen a fast scanning-pulse GC analysis, FASPA, a technique analogous to the step-scan technique in IR spectroscopy [26] and based on a series of repetitive MeOH pulse injections combined with GC product analysis. To achieve the fine synchronization between MeOH pulse injection and the GC sampling, a Labview program was designed, which allows to control the following parameters during the experiment: (i) the switching of a six-way valve to achieve the repetitive

injection of MeOH pulses to the reactor with a pre-set pulse interval; (ii) after each MeOH pulse, a GC product sample was taken after a controlled delay time. Importantly, the time delay of each GC sampling was step-wise increased from zero to the end of the pulse time (taken to be the GC analysis time) to record the temporal product response information upon the MeOH pulse. The delay time step is adjustable during the operation to modify the time resolution of product responses in some specified periods. After the completion of the test, all GC points are collected to build up the full map of quantitative product responses after a MeOH pulse. The FASPA test protocol is illustrated in Fig. 1.

In a typical FASPA experiment in this study, an initial time delay of 1 s was chosen for GC sampling when the MeOH pulse interval is 3.75 min. In a later stage, the time step is increased to 4 s when changes in product concentrations are lower. In total, a sequence of 65–165 GC sample injections (corresponding to 130–330 pulses of MeOH) depending on different reaction conditions (Table 1) were collected to reconstruct the whole temporal product profiles of a MeOH pulse. Very recently, a similar concept of (un)synchronizing GC sampling and reactant pulsing was employed by Kosinov *et al.* with a so-called scanning pulse reaction technique for transient kinetic analysis [27]. In their approach, GC acquisition and reactant pulsing were collected both in a repeating manner without the fine time-delay control program as used in the FASPA technique. To compare, the time span between two adjacent GC samplings ( $t_{\text{delay}}$  in Fig. 1(b)) may be set even  $< 1$  s, which can be also adjusted during the test thanks to the used time control program in the FASPA approach in this study.

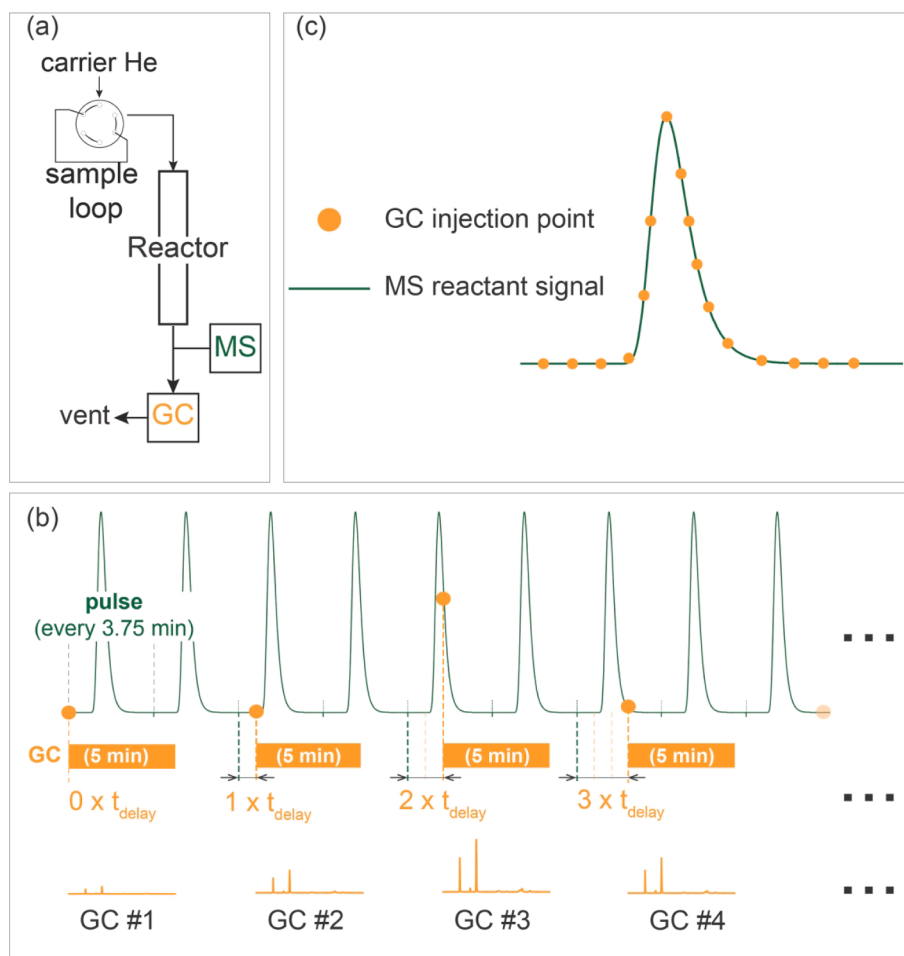


**Fig. 1.** Overview of the FASPA approach. (a) A flow scheme of FASPA setup; (b) Normalized MS reactant signal and GC injections in a typical FASPA experiment. The MeOH pulse interval and time delay of GC sampling are initially set in the control program; (c) Normalized mapping of a typical FASPA experiment after collection of all GC points.

**Table 1**  
Quantitative experimental data of stimulus–response experiments.

Sample mass (mg)	200	100	50	4.5		
#BAS sites (μmol)*	104	52	26	2.3		
Pulse size (mL)	0.25	0.25	2	0.25	0.25	2
(μmol)**	1.21	1.21	7.6	1.21	1.21	7.6
MeOH/BAS (mol/mol)	0.012	0.023	0.146	0.047	0.526	3.304
# Pulses used***	165	134	140	152	65	143

\*: BAS concentration was measured by FTIR spectroscopy using pyridine as probe at 160 °C.

\*\* : The MeOH concentration in all pulses was 12 and 9 vol% in helium in 0.25- and 2.0-mL sample loop, respectively.

\*\*\*: Total # pulses used for reconstruction of a methanol pulse response composition by fast scanning-pulse GC analysis.

### 2.3.2. Product analysis-Gas chromatography

A Thermo Trace GC with two individual channels was connected downstream of MS (Fig. 1(a)). One channel is equipped with an RTX–1 column (2 m, 0.32 mm, 5.00 μm) and Al<sub>2</sub>O<sub>3</sub>/KCl column (15 m, 0.32 mm, 10 μm) connected to a flame ionization detector (FID) for the analysis of C<sub>1</sub> to C<sub>4</sub> hydrocarbons. The other is equipped with an RTX-VMS column (30 m, 0.33 mm, 3.00 μm) also connected to an FID for C<sub>5+</sub> hydrocarbons analysis. Examples of GC chromatograms collected from the two separate channels are shown in Fig. S2. Since the GC is located downstream of the MS a synchronization delay of 2–4 s is observed for GC analysis. Therefore, MS signals were adjusted to the GC-pulse analysis timing by adding a time difference based on the breakthrough time difference between *m/z* = 41 and 40 in MS.

The MeOH + DME (dimethyl ether) conversion, selectivity and yield were then calculated on a carbon molar basis as follows:

$$X = (\phi_{C,MeOH_{in}} - \phi_{C,MeOH_{out}} - 2\phi_{C,DME_{out}}) / \phi_{C,MeOH_{in}} \times 100\% \quad (3)$$

$$S_{Cn} = n \cdot \phi_{Cn} / (\phi_{C,MeOH_{in}} - \phi_{C,MeOH_{out}} - 2\phi_{C,DME_{out}}) \times 100\% \quad (4)$$

$$Y_{Cn} = \frac{X \times S_{Cn}}{100} \quad (5)$$

where *X*,  $\phi_{Cn}$ , *S<sub>Cn</sub>*, and *Y<sub>Cn</sub>* represent the carbon-based conversion of MeOH plus DME, molar flow rate, carbon selectivity to a certain hydrocarbon product with carbon number equal to *n* and the corresponding carbon yield, respectively.

### 2.3.3. Statistical moments analysis of pulse data – turn-over frequency

The interpretation and data analysis of the temporal pulse responses are based on the statistical moment analysis of the response curve from FASPA experiments upon injection of a tracer pulse [28,29].

The normalized *n*<sup>th</sup> absolute moment on the origin of a response is defined as:

$$\mu_n = \frac{\int_0^\infty t^n c(t) dt}{\int_0^\infty c(t) dt} \quad (6)$$

here *c(t)* is the concentration of tracer at the outlet as a function of time-stream upon a pulse injection.

And the normalized *n*<sup>th</sup> central moment on the mean as:

$$\mu'_n = \frac{\int_0^\infty (t - \mu_1)^n c(t) dt}{\int_0^\infty c(t) dt} \quad (7)$$

Both are normalized by the amount of tracer injected *N<sub>inj</sub>* (mol), the 0<sup>th</sup> moment, and have the dimension of time.

$$\mu_0 = \int_0^\infty c(t) dt = N_{inj} \quad (8)$$

The normalized first moment represents the average residence time  $\tau$  in the system:

$$\mu_1 = \frac{\int_0^\infty t \cdot c(t) dt}{\int_0^\infty c(t) dt} = \tau \quad (9)$$

The normalized second central moment represents the variance  $\sigma^2$  of the response curve:

$$\mu'_2 = \frac{\int_0^\infty (t - \tau)^2 c(t) dt}{\int_0^\infty c(t) dt} = \sigma^2 \quad (10)$$

The third moment is a measure of the asymmetry or skewness of the response curve, but in most studies, only the 1<sup>st</sup> moment and 2<sup>nd</sup> central moment are analyzed since the weight of the tail of a response signal increases with *t*<sup>*n*</sup>, whereas the accuracy of that tail signal usually diminishes.

For Gas-Solid Chromatography analysis Kubín and Kučera derived expressions for the moments of the response curve of a tracer pulse injection to a 1-dimensional packed bed of porous particles, taking into account the axial dispersion in the packed bed, mass transfer to and diffusion into the porous particles, and linear adsorption–desorption at the particles' surface [30–36]. For small injection amounts the Henry regime applies for adsorption. This is the basis for our analysis of the pulse responses.

The normalized first moment consists of contributions from the residence time spent in the gas phase of the system under consideration (tubings, represented by  $\tau_{set-up}$ ), in the packed bed (interparticle and intraparticle space, represented by  $\tau_{interparticle}$  and  $\tau_{intraparticle}$ , respectively), and the residence time spent in the adsorbed state ( $\tau_{ads}$ ):

$$\mu_1 = \tau_{set-up} + \tau_{interparticle} + \tau_{intraparticle} + \tau_{ads} \quad (11)$$

$$\mu_1 = \tau_{set-up} + \frac{L_b}{u} [\varepsilon_b + (1 - \varepsilon_b)\varepsilon_p + (1 - \varepsilon_b)\rho_p K_A] \quad (12)$$

here *L<sub>b</sub>* is the length of the catalyst bed, *u* is the superficial velocity of carrier flow in the reactor,  $\varepsilon_b$  and  $\varepsilon_p$  represent the external bed porosity and internal pellet porosity, respectively, of the catalyst bed packed with zeolite pellets, and  $\rho_p$  is the particle density.

It is noted that only the adsorption term appears in the expression for the first moment of a nonreactive system (Eq. (12)). In this work, only the zeroth and first moments are used. This expression can further be simplified for cases with specific assumptions (e.g. non-porous particles, or no adsorption etc.).

In case a non-ideal Dirac tracer pulse is used (e.g. a Gaussian or a block pulse [37]) the first moment satisfies the relation (Eq. (13)), so the 'true' moment of the system can be obtained by taking a proper (e.g. non-adsorbing) tracer response as input reference, in our case from the argon injected together with the species under investigation (*vide infra*). This corrects for the non-ideal pulse shape and at the same time eliminates the residence time in the system and the bed and particle porosities.

$$\mu_1 = \mu_{1,response} - \mu_{1,input} \quad (13)$$

For a nonreactive adsorbing component holds then:

$$\tau_{ads,HC} = \mu_{1,HC} - \mu_{1,Ar} \quad (14)$$

$$\tau_{ads,HC} = \frac{L_b}{u} [(1 - \varepsilon_b)\rho_p K_A] \quad (15)$$

These first moments are also used to estimate the minimum turn-over frequencies for the products' formation, *TOF<sub>prod</sub>*. For this purpose, the maximum number of active sites involved, *N<sub>act</sub>*, is equated to the number of MeOH molecules pulsed (see Table 1), although this will be still an overestimation.

The characteristic hydrocarbon product formation time  $\tau_{prod,HC}$  is the first moment of the specific product minus that of argon for the hydrocarbons to account for the system delay over H-ZSM-5, and comprises the characteristic times of adsorption and of the formation process(es) of the component under consideration.

$$\tau_{prod.HC} = \mu_{1,HC} - \mu_{1,Ar} = \tau_{adsorption} + \tau_{formation} \quad (16)$$

$$TOF_{prod} \geq \frac{N_{prod}}{\tau_{prod} N_{act}} \quad (17)$$

For first-order reaction systems, Chan *et al.* showed that the statistical method of moments can be applied to determine the rate constants of individual reactions from the transient batch reactor operation, being the reciprocal of the  $\tau_{formation}$  [38]. Since the  $\tau_{adsorption}$  in (Eq. (16)) is not known, the estimated TOFs by (Eq. (17)) are lower limit estimates. Also for the pulse-response analysis in the TAP reactor system [39], based on diffusive transport, moments-based relations have been derived to extract kinetic information [40,41]. The derivation of the kinetic relations follows a slightly different approach, but the first moment relation for a non-reactive system is identical to that for the adsorption-desorption process in packed beds presented above. The TAP system has recently been used for the analysis of light alkene reactions over H-ZSM-22 [20]. In the figures the time-corrected MS response of the argon tracer, injected together with the MeOH, has been included.

The two-peak response of the light aromatics (benzene, toluene and xylenes) were deconvoluted by fitting the exponentially modified Gaussian (EMG) peak function GaussMod, used in chromatography:

$$f(x) = y_0 + \frac{A}{t_0} e^{\frac{1}{2} \left( \frac{w}{t_0} \right)^2 - \frac{x-x_c}{t_0}} \int_{-\infty}^x \frac{1}{\sqrt{2\pi}} e^{-\frac{y^2}{2}} dy \quad (18)$$

with.

$$z = \frac{x - x_c}{w} - \frac{w}{t_0} \quad (19)$$

here  $y_0$ ,  $A$ ,  $w$ ,  $x_c$  represent offset, area, full width at half maximum and center of the response.  $t_0$  is used to estimate the first moment of the response,  $\mu_1 = x_c + t_0$ .

#### 2.3.4. In situ DRIFT spectroscopy measurement

*In situ* Diffuse Reflectance Infrared Fourier Transformed (DRIFT) spectra were recorded using a Nicolet Magna 550 spectrometer, equipped with a liquid-nitrogen-cooled MCT detector and a Praying Mantis diffuse reflection accessory (Harrick Scientific) with a high-temperature reaction chamber. The temperature is controlled via the thermocouple under the sample. To mitigate the impact of water on spectra measurement, MeOH is replaced by DME (25 vol% in  $N_2$ ) as a reactant. The flow of gases was controlled by mass flow controllers (Bronkhorst). ~10 mg H-ZSM-5 in powder form was loaded in the reaction cell equipped with  $CaF_2$  windows. Prior to the measurements, sample powders were exposed to an air flow (10 mL<sub>NTP</sub>/min) at 400 °C for 1 h. Subsequently, the system was cooled to 300 °C for reaction. DME was dosed via the six-way valve with a sample loop (~10 mL). The corresponding pulse quantity is 0.2 mmol<sub>C</sub> per pulse. 20 mL<sub>NTP</sub>/min He was used as the carrier gas. The pulse interval is 2.5 min. The spectra were acquired every 4 s to follow the pretreatment, reaction, and evolution of surface species within 4000–1400  $cm^{-1}$  with a resolution of 4  $cm^{-1}$ . In particular, characteristic IR bands within 1700–1400  $cm^{-1}$  assigned to various aromatic surface species are summarized in Table S1.

### 3. Results and analysis

#### 3.1. Fast Scanning-Pulse analysis (FASPA) validation

The basic condition for the applicability of FASPA is that during this sampling process the system under study does not change, which can be verified by operating at reference conditions before and after the sampling process. To verify the catalyst bed performance is neither changed nor approaching deactivation during the entire pulse sequence, a continuous MTH operation test was carried out before and after the entire pulse sequence. The obtained steady-state product distributions from GC before and after the pulse sequence are then compared in Fig. 2.

> 540 pulses were injected in this test, which in total equals to 1.3 mol MeOH per mol of BAS (Brønsted acid sites). MTH data in a continuous MTH test reveal that this H-ZSM-5 catalyst can convert > 11000 mol MeOH per mol of BAS before MeOH conversion drops below 100 % at 400 °C. The catalytic results (Fig. 2(a)) show that the product selectivity is not changed after the FASPA test. A dark grey zone indicating coke deposition mainly at the top of the catalyst bed can be observed (Fig. 2(b)) after the entire experiment [17]. So, the basic condition for the application of FASPA in the MTH process is satisfied. As shown in Fig. 2(c), the MS signal of  $m/z = 41$ , qualitatively representing light hydrocarbon (*e.g.*, propylene, butylenes, butanes) production in the FASPA test, reaches a *quasi* steady-state profile within ~10 MeOH pulses until the end of the test. A second proof justifying the FASPA application condition follows from the preservation of the temporal product responses (ethylene, propylene, butanes, and xylenes) of two consecutive FASPA sequences (Fig. 2(d)). The systematic sampling order could possibly have introduced a systematic error in the response profiles. However, the asynchronous MeOH pulsing and GC sampling in the recent paper of Kosinov *et al.* [27], implying a random collection of data points, yielded similar product response profiles, *e.g.*, the two production profiles of the aromatic species shown in Fig. 3.

Therefore, we conclude that during the FASPA test the catalyst bed is at *quasi* steady-state conditions providing a constant product distribution in the exit flow. So, the FASPA technique can be safely applied as a characterization method without disturbing a consecutive continuous steady-state MTH operation. Furthermore, in comparison with the TAP reactor, the FASPA approach is relatively cheap and allows investigation of the catalyst bed performance at typical operating temperatures (*e.g.*, > 400 °C) in standard catalyst testing equipment.

#### 3.2. Varying reaction temperature

The FASPA experiments were first conducted over 100 mg H-ZSM-5 at 390–420 °C. The full temporal responses are present in Fig. 3. More plots and corresponding moment analysis (zeroth and first moments) and selectivity can be found in Fig. S4–S5 and Table S2.

At the studied conditions, the amount of MeOH in the pulse is far less than the BAS concentration in the catalyst bed (~2 % of BAS for 100 mg H-ZSM-5 and 0.25 mL loop, see Table 1), resulting in the complete conversion of MeOH. A nearly instantaneous formation of hydrocarbons (alkanes, alkenes, and light aromatics) is observed after 2.8–4.7 s delay depending on the reaction temperature after the argon response. The latter represents all non-adsorption and non-reaction phenomena in the setup [31,33,42]. The major alkane and alkene responses are the butanes (predominantly isobutane) and propylene, followed by ethylene and butylenes. Especially alkenes show more tailing than the argon response, further evidenced by the higher first moments of alkenes than of alkanes seen in Table S2. This indicates a longer formation duration of alkenes at the sample.

The time difference between Ar and hydrocarbon breakthrough ascribed to the induction period prior to the first hydrocarbon formation significantly drops from > 4 s at 390 °C to 2.8 s at 420 °C (Fig. 3), demonstrating a faster HCP build-up at higher reaction temperature under the same conditions [14,43]. However, the impact of temperature on the selectivity (Table S2) of aliphatics is less pronounced than that on light aromatics in this narrow temperature range. With increasing temperature, the selectivity to light alkanes including methane, ethane and propane is monotonically increased, as a result of the promoted cracking of heavier hydrocarbons [44–46]. The small rise of ethylene and propylene with temperature at the expense of butylenes and  $C_{5+}$  aliphatics might indicate that increased temperature promotes the earlier cracking of heavier hydrocarbons into shorter olefins, *i.e.*, ethylene and propylene [14,47].

Interestingly, the order of magnitude lower production of light aromatics (benzene, toluene, xylenes (BTX) in Fig. 3) is a convolution of a fast formation on the time scale of the aliphatics formation (denoted as

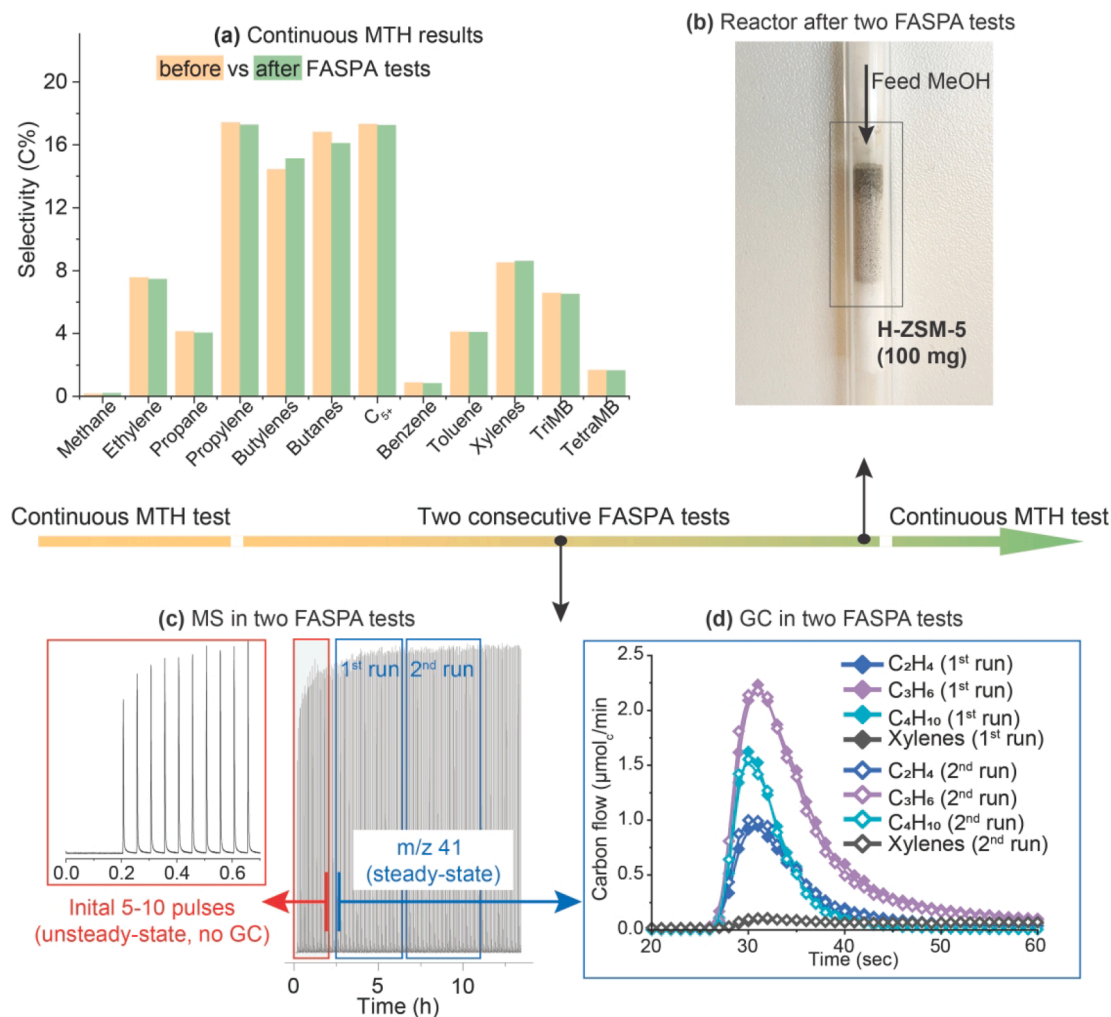


**Fig. 2.** (a) Carbon selectivity in continuous MTH operation before and after the FASPA tests; (b) instant view of the reactor after  $\sim 540$  MeOH pulses; (c) MS signal of  $m/z = 41$  representing light hydrocarbons along time during the FASPA test; (d) GC temporal responses of selected hydrocarbons in two consecutive FASPA tests. Reaction conditions:  $T = 400$  °C,  $m_{\text{cat}} = 50$  mg (150–212  $\mu\text{m}$ ),  $P_{\text{reactor}} = 1$  bar,  $WHSV = 226$  mol<sub>C</sub> mol<sub>B</sub>As<sup>-1</sup>h<sup>-1</sup> in continuous MTH test, MeOH pulse quantity = 1.2  $\mu\text{mol}_C$  per pulse, carrier gas He = 20 mL<sub>NTP</sub>/min, pulse interval = 3 min,  $t_{\text{delay}} = 1$  s. More MS results can be found in Fig. S3.

R1) and a slower second formation over a longer period (denoted as R2). The similar peak locations of R1 at 35–40 s as the BTX pulse responses for adsorption presented in Fig. S11 also suggest the almost instantaneous formation of aromatics before 40 s followed by a long tail ascribed to the rather slow desorption of BTX at 400 °C after 40 s. Unlike BTX responses, TriMB does not exhibit the two-peak profile implying no slower formation of TriMB in the later stage ( $> 60$  s) of the pulse response. Furthermore, characteristic IR bands, assigned to different cyclic HCP species (cyclopentenyl species and methylated benzenes shown in Fig. 4 with detailed IR assignments found in Table S1), also reach their maximum at  $\sim 30$  s. After that, their intensities slowly return to zero without the secondary peak as observed for BTX responses in FASPA tests (Fig. 3). No net increase in IR signal intensity level after a complete pulse (Fig. 4) also indicates that a *quasi* steady-state MTH pulse activity is attained. The close correlation between IR bands and product responses suggests a dynamic rather than a static HCP as reservoir of active species where MeOH is converted into hydrocarbons [15,48]. The involved surface species are highly reactive and unstable. They are rapidly formed but also subsequently completely decomposed, as indicated by IR bands during the pulse, releasing final products. Compared to the formation, the decomposition of HCP species is relatively slow. Based on the IR assignments from literature [49–59] (see Table S1), we speculate these pool species are mainly alkylated mono-/di-/trienyl carbenium ions (1465, 1480–1510  $\text{cm}^{-1}$ ) such as cyclopentenyl

carbenium ions and alkylbenzenes (1456, 1591, 1616  $\text{cm}^{-1}$ ), with the latter being the result of deprotonation and cycle expansion processes of the former [60]. Their rapid formation and slow decomposition are well in line with reported <sup>13</sup>C CP-MAS NMR results that 1,3-dimethylcyclopentenyl carbenium ions were detected in  $< 1$  s after pulsing ethylene, while their transformation into methylbenzenes (predominantly pentamethylbenzenes [61]) took seconds at 350 °C [23,24]. The reduced time difference between Ar tracer and the breakthrough of hydrocarbons with reaction temperature (Fig. 3) implies that this transition process, *i.e.*, induction until the completion of HCP at the presence of MeOH can be sufficiently accelerated by elevating reaction temperature from 390 to 420 °C.

For the temperature impact on BTX formation, the location of the R1 component (sharp) of all aromatic species is consistently located near 40 s, a few seconds later than the Ar reference response, whereas its amount decreases with increasing temperature. Moreover, the R2 component (broad) virtually increases and shifts towards earlier response times at higher temperature, ascribed to a faster (activated) decomposition/and release of HCP species after MeOH being depleted.

Additional mechanistic information lies in the earlier appearance of methane prior to other hydrocarbons (see 400 °C in Fig. 3 and an enlarged view in Fig. S5), which helps to link the possible first C–C formation mechanism prior to the subsequent steady-state formation of hydrocarbons. Methane is readily formed  $\sim 1$  s earlier than other

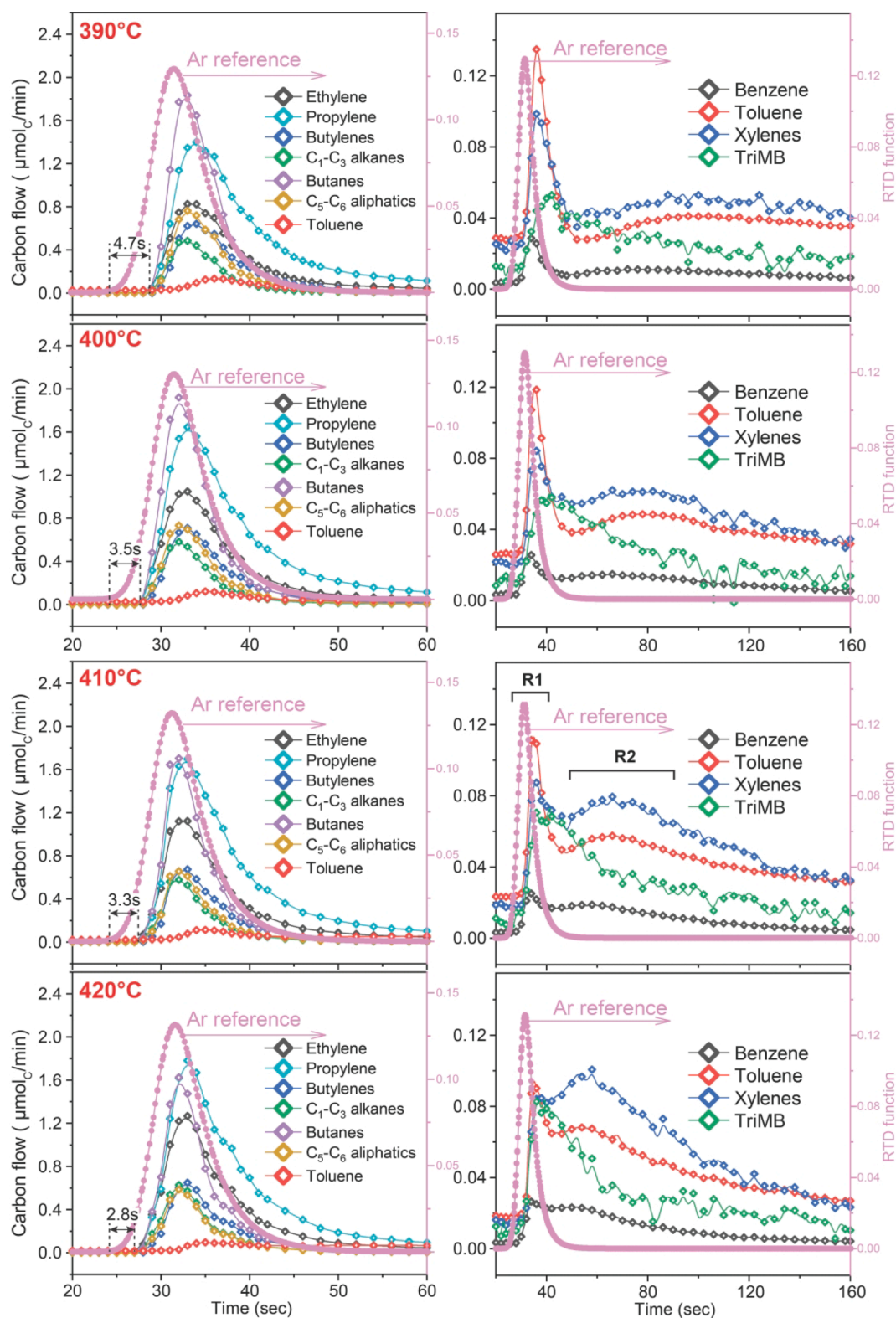


**Fig. 3.** Hydrocarbons responses upon pulsing MeOH over H-ZSM-5 at 390–420 °C. Conditions:  $m_{\text{cat}} = 100$  mg (H-ZSM-5, Si/Al 25, 150–212  $\mu\text{m}$ ),  $P_{\text{reactor}} = 1$  bar, MeOH pulse quantity = 1.2  $\mu\text{mol}_C$  per pulse, carrier gas He = 20  $\text{mL}_{\text{NTP}}/\text{min}$ , pulse interval = 3.75 min.

aliphatics, although in much smaller quantities. Recently proposed first C–C bond formation mechanisms such as the CO [62–64]/formaldehyde [65]-mediated or extraframework alumina-assisted [66] routes involve the formation of methane as a side product in the MeOH decomposition or disproportionation reactions [12]. After the rapid formation of hydrocarbons giving the response over 20–40 s, methane

exhibits a longer tailing than other alkanes (Fig. 3 and Fig. S5), while the latter species are believed to be the side products of hydrogen-transfer reactions [67] eventually leading to aromatics formation with alkylated cyclopentenyl ions as intermediates [23,49,61,68]. Beyond 60 s response time, the further (secondary) reactions such as (mono-molecular) cracking [69] of those highly alkylated cyclic or methylated

aromatic species give the second broad peak of light aromatics and the long tail of methane.

In brief, upon a MeOH pulse aliphatics and aromatics are nearly instantaneously formed after a short induction period, which can be significantly shortened at the elevated temperature. At later response times, tailing alkene responses and a second appearance of BTX is observed spread over a broad time range, and tentatively attributed to the slow decomposition of retained surface species. At these reaction conditions, the MeOH pulse only probes  $\sim 2\%$  of the BAS, so a very thin reaction zone is active in the catalyst bed, responsible for the fast primary products formation.

### 3.3. Varying catalyst loadings

To explore more insights on the origins of the secondary formations of BTX, FASPA experimental results over H-ZSM-5 catalysts samples of 4.5–200 mg were compared. The output of a smaller sample can be considered as input for the downstream region of a larger sample. Accordingly, the additional changes in responses for larger catalyst samples must be due to secondary reactions in that downstream region of the bed. Results are presented in Figs. 5–6 and the quantities of individual components in Table S3.

With increasing catalyst sample from 4.5 to 200 mg, the observed formation of C<sub>5</sub>–C<sub>6</sub> aliphatics gradually decreased, while aromatics and C<sub>1</sub>–C<sub>4</sub> alkanes simultaneously increased, indicating the H-transfer and aromatization from heavier aliphatics to aromatics continue in the downstream region of the catalyst bed in absence of MeOH, eventually increasing the selectivity to aromatics [19,70,71]. Similarly, olefins also decrease in the catalyst with longer beds, indicating olefins are further converted in these regions. The selectivity to propylene and butylenes decreases, while that to ethylene increases with sample amount. The increasing alkanes production is mainly due to the butanes.

The lower selectivity to aromatics for the 200 mg sample is attributed to residual aromatics still adsorbed in this sample at the end of the pulse. The MeOH pulse injection time interval is slightly too short for full desorption from this sample. The lower carbon balance of  $\sim 0.9$  for this 200 mg catalyst also suggests  $\sim 0.1 \mu\text{mol}$  carbon (probably in form of aromatics) remained still on the surface when a next pulse injection was given.

With decreasing catalyst amount, both R1 and R2 components (representing the fast and slow BTX formation, as denoted in Fig. 3) appear at shorter residence time. For the shortest catalyst bed with only 4.5 mg catalyst, R2 of BTX is almost absent suggesting the slow formation of BTX does not take place in the presence of MeOH [46].

For the 4.5 to 200 mg catalyst samples, the only difference is the

downstream catalyst region since MeOH is rapidly consumed forming the identical surface species (cyclopentenyl species and methylated benzenes, see *in situ* DRIFT results in Fig. 4) at the entrance region of the catalyst bed in the pulse experiments. In Section 3.2, we concluded that R2 stems from the slow desorption/decomposition of strongly adsorbed surface species, evidenced by the slow decreasing intensity of characteristic IR bands. However, the R2 response over 4.5 mg H-ZSM-5 is almost completely absent at full MeOH conversion. Furthermore, the component distribution of all responses (selectivity and zeroth moments, see Fig. 6 and Table S3) varies with catalyst mass. All these observations cannot be solely explained by the slow desorption/decomposition of surface species. It must suggest that besides the desorption/decomposition of surface species, secondary reactions like H-transfer and aromatization reaction also contribute to the second aromatics formation. Especially the long tailing of propylene for all catalysts and the much higher formations of propylene and C<sub>5</sub>–C<sub>6</sub> aliphatics over the shortest 4.5 mg bed than over larger samples are strong indicators. Accordingly, two distinct aromatization pathways are discerned in the FASPA experiments. The MeOH-mediated aromatization proceeds quickly giving component R1. After that, secondary reactions including slow decomposition of surface species and H-transfer reactions (probably from propylene/butylenes and also C<sub>5</sub>–C<sub>6</sub> aliphatics) result in a broad BTX formation referred to as R2 at later stages.

### 3.4. Varying injection amount

To evaluate the impact of MeOH on the product temporal responses, in particular when the MeOH conversion is below 100 %, FASPA experiments were compared for two pulse sizes (1.2 and 7.6  $\mu\text{mol}_C/\text{pulse}$ ) over 4.5 mg H-ZSM-5 at 400 °C and results were shown in Fig. 7. The full map of product responses and quantitative moment estimates can be found in Fig. S6 and Table S4.

With the larger pulse size of 7.6  $\mu\text{mol}_C$ , the MeOH conversion is  $\sim 95\%$ . In that case, The response time delay between argon and products has almost completely disappeared, evidenced by the narrower time span between MS signals  $m/z$  40 and 41 in FASPA tests in Fig. 7(a). Accordingly, MeOH is available across the entire catalyst bed with the larger pulse size in the FASPA test, MTH reactions proceed towards bulkier hydrocarbons resulting in the higher selectivity to C<sub>5+</sub> aliphatics and aromatics (BTX and TriMB) mainly at the expense of propylene (Fig. 7(b and c)). For the BTX response in Fig. 7(d), ascribed to the suppressed secondary reactions (such as hydrogen transfer reactions) at the presence of MeOH two BTX formations peaks were completely convolved into one broad peak sitting at  $\sim 35$  s, just after the aliphatic responses (Fig. S6).

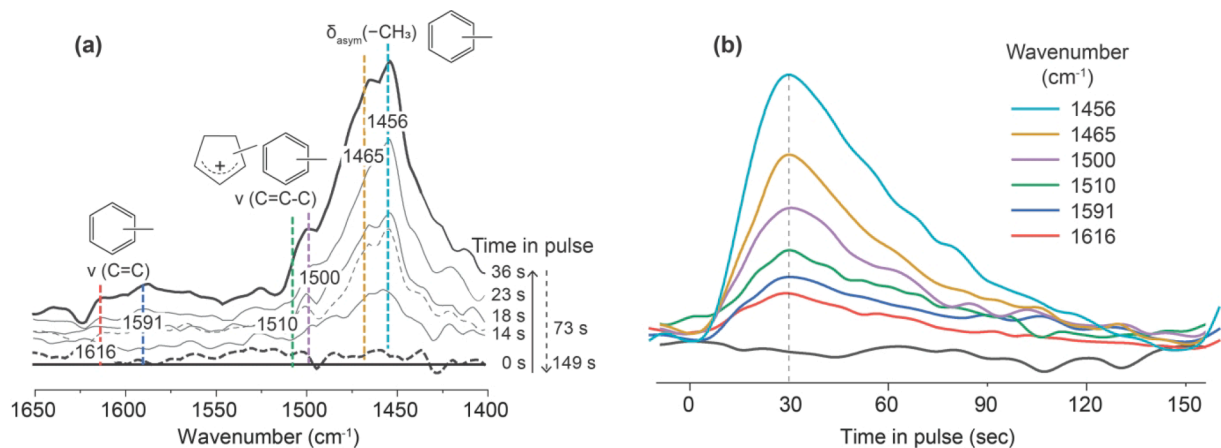


**Fig. 4.** Temporal evolution of DRIFT spectra in the 1650–1400  $\text{cm}^{-1}$  region (a) and the changes of characteristic IR bands along time (b). *In-situ* DRIFT experimental conditions:  $T = 300\text{ }^\circ\text{C}$ ,  $m_{\text{cat}} = \sim 10\text{ mg}$  (H-ZSM-5, Si/Al 25, powder form),  $P_{\text{reactor}} = 1\text{ bar}$ , pulse quantity 0.2  $\text{mmol}_C$  per pulse, carrier gas He = 20  $\text{mL}_{\text{NTP}}/\text{min}$ , pulse interval 2.5 min. To mitigate the impact of water on the IR signal, DME (23 vol% in  $\text{N}_2$ ) was pulsed instead of MeOH.

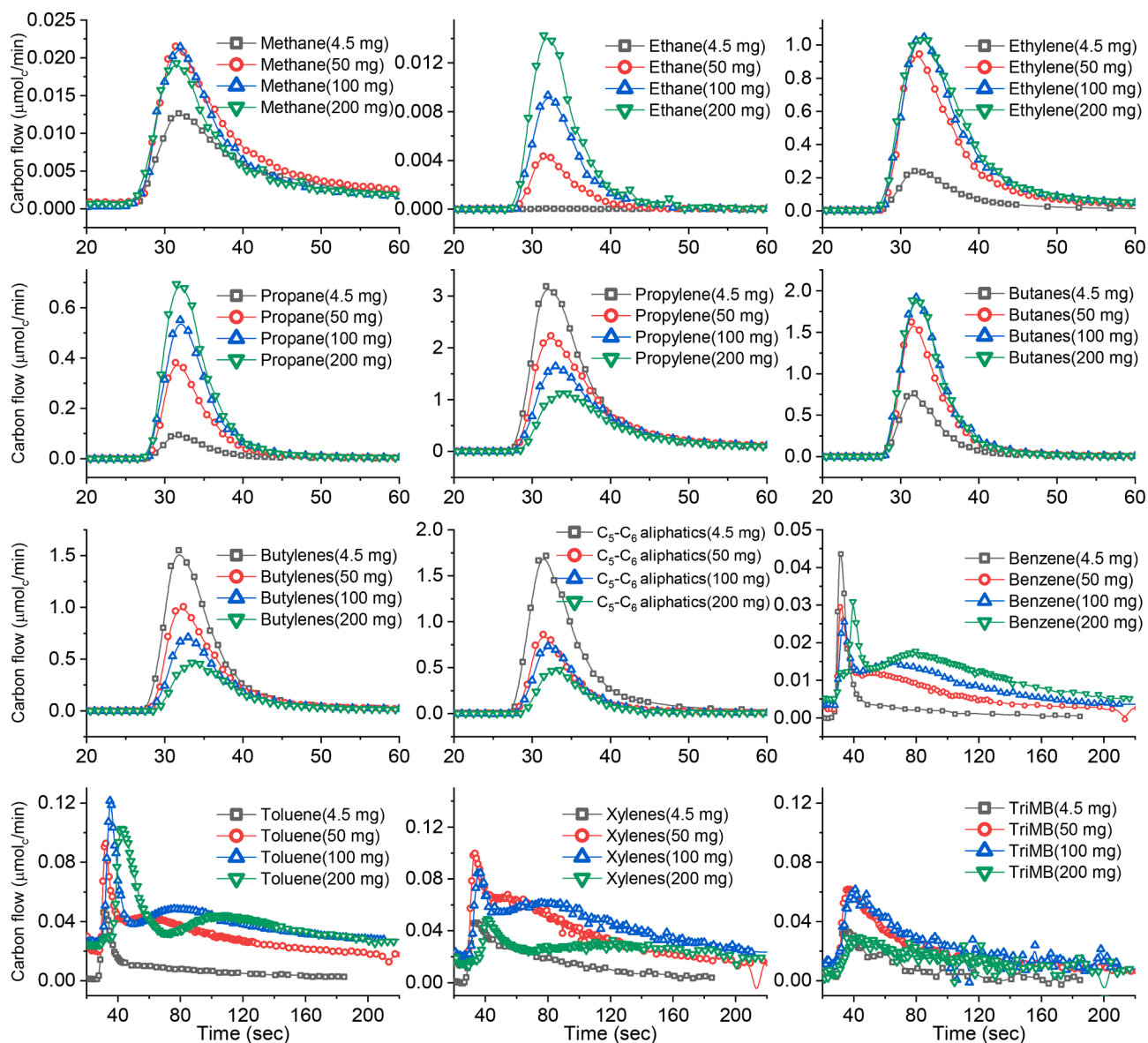


**Fig. 5.** Comparison of hydrocarbons responses upon pulsing MeOH over 4.5–200 mg H-ZSM-5 at 400 °C. Conditions: H-ZSM-5 (Si/Al 25, 150–212  $\mu\text{m}$ ),  $P_{\text{reactor}} = 1$  bar, MeOH pulse quantity = 1.2  $\mu\text{mol}_C$  per pulse, carrier gas He = 20 mL<sub>NTP</sub>/min, pulse interval = 3.75 min. More quantitative experimental data can be found in [Table S3](#). Response profiles were time-shifted based on the Ar response using 100-mg H-ZSM-5 sample as reference.

At the incomplete MeOH conversion level, the estimated zeroth and first statistical moments for 4.5 mg H-ZSM-5 with 7.6  $\mu\text{mol}_C$  per pulse help to calculate the minimum turn-over frequencies (Eq. (17)) assuming BAS as the active site in the induction period and the autocatalysis process once fully developed. The real product formation rates must be higher than the reported values in [Table S4](#), since the adsorption/desorption increase the residence time (first moment,  $\mu_1$ ) of hydrocarbons. The estimated minimum turn-over frequency of propylene is 0.44  $\text{mol}_C/\text{mol}_{\text{BAS}}/\text{s}$ , in good agreement with the reported range of 0.24–1.8  $\text{mol}_C/\text{mol}_{\text{BAS}}/\text{s}$  at 400 °C [71,72] confirming the feasibility of conducting a kinetic investigation of MTH reactions through the FASPA experiment. Moreover, FASPA experiments carried out at industrially relevant conditions (i.e., high reaction temperature) provides unprecedented and quantitative results for a kinetics study in complex reaction systems. In combination with variation of residence time further insight in reaction pathways can be revealed.

#### 4. Discussion

The objective of this study is to introduce and validate a newly developed fast scanning-pulse analysis (FASPA) technique with GC quantification under varied reacting conditions and demonstrate its applicability to shed light on reaction pathways in the complex network of the MTH process on a working H-ZSM-5 catalyst under industrially-relevant conditions.

The experimentally validated FASPA approach ([Figs. 1-2](#)), allows the quantitative mapping of the product spectrum response upon a small reactant pulse with a high time resolution, even when the GC analysis time is much larger than the pulse response. In the presented quantitative results seconds resolution is easily achieved for the full spectrum of gaseous products in the MTH over H-ZSM-5, achieved with a relatively cheap instrumentation, something that is even beyond reach with advanced instrumentation like the TAP system, TOF-MS analysis or Spaci-MS operation due to the reliance on MS analysis [20,62,73,74].

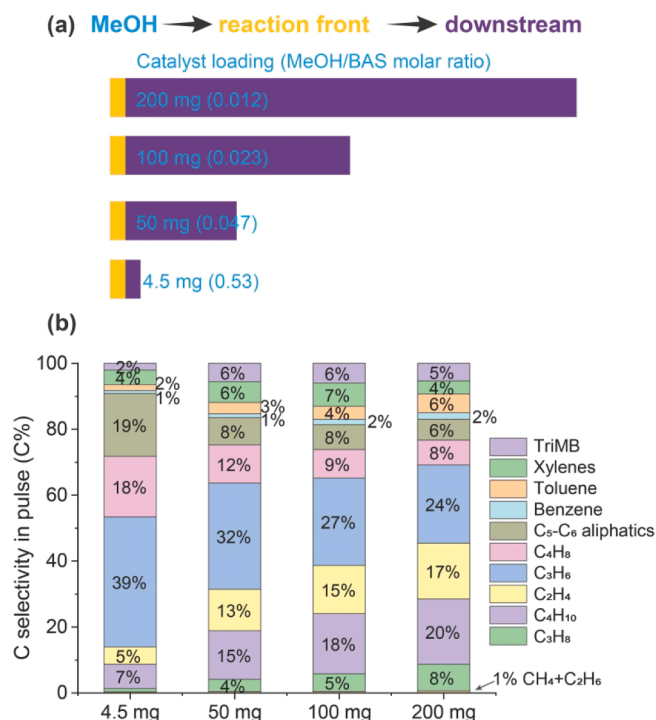


Fig. 6. (a) The length of the downstream region of the bed affected by varying catalyst loadings (4.5–200 mg); (b) total carbon selectivity of hydrocarbons over H-ZSM-5 with varied loadings in the FASPA experiments. Other FASPA conditions are as in Fig. 5.

The quantitative data interpretation is based on the statistical moments analysis [28,29], that has been applied extensively for transient non-reactive gas–solid chromatography established by Kubín and Kučera [31–36,42,75] and greatly used since 1970 s. Later this has been extended to reactive transient data of batch and pulse reactors [38,40,41]. The pulse-response technique combined with moment analysis for the investigation of hydrocarbons adsorption on zeolitic materials (see Fig. S8–S12), demonstrates the applicability of this approach to a packed bed reactor system in this study, and provides the basis of the current study of the MTH process over H-ZSM-5 catalyst under reaction conditions. In this study only the zeroth and first moment are used. The use of an inert tracer (argon) is essential to account for set-up contributions [76,77]. The moments analysis then provides information about the adsorption–desorption behavior and rate parameters (turn-over frequencies, *TOFs*) of MTH species. This approach could provide kinetic information on the formation of individual products (cf. Table S4) to bring us closer to a more quantitative understanding of this complex process [16]. The apparent adsorption enthalpies of BTX estimated using a Van ‘t Hoff relation (Table S5–S6) are well in line with the wide range of values reported in literature [78–85]. The evident temperature influence on BTX adsorption on H-ZSM-5 implies that the quick MeOH conversion and hydrocarbon formation rates are tightly associated with thermodynamics of sluggish BTX adsorption–desorption processes, particularly at temperatures below 400 °C. Packed bed reactors therefore behave spatially as chromatographic reactors, making kinetic examination of the MTH process in the zeolite catalyst at lower temperatures challenging [17,86].

This study represents a showcase of the FASPA approach applied to study the MTH process by conducting experiments on different amounts of a model H-ZSM-5 catalyst at 390–420 °C with the pulse size of 1.2 and 7.6  $\mu\text{mol}_C$ , covering both temporal and spatial compositions. Through the analysis of the product response of MeOH pulses to an active H-ZSM-5 catalyst the genesis of hydrocarbon pool species in the induction period, their dynamics during autocatalytic formation of reaction

products in the transition period, and their final decomposition could be followed. Specifically, two different aromatization routes at operating conditions were observed.

Temperature has an evident effect on the time delay between Ar and hydrocarbons demonstrating the induction period for the HCP build-up/restoration can be greatly shortened when temperature is just increased by 30 °C from 390 to 420C. Besides, methane is observed about 1 s prior to other hydrocarbons, which may be associated to the first C–C bond formation by CO [62–64]/formaldehyde [65]-mediated or extra-framework alumina-assisted [66] pathways with methane formation as a byproduct in the induction phase. Temperature also affects the first and second aromatic responses, yet the overall selectivity to aromatics increases slightly as the temperature rises from 390 to 420 °C (Table S2). First, higher temperatures accelerate the desorption of aromatics, resulting in a cleaner zeolite surface prior to the next MeOH pulse, as seen by the lower BTX baselines in Fig. 3. Secondary processes, such as hydrogen transfer, cyclization, aromatization and desorption, are preferred at higher temperatures once MeOH is depleted, resulting in the 2<sup>nd</sup> BTX response moving to a shorter response time and increasing intensity leading to the increasing selectivity to the secondary formation of BTX (R2) after pulse time of 60 s, which specifically occurs in the downstream region of the catalyst bed [87].

In the MeOH pulse experiment over 4.5 mg catalyst the conversion is just complete when using the pulse size of 1.2  $\mu\text{mol}_C$ , so its product response composition is input to the rest of the catalyst bed for the larger sample (50–200 mg H-ZSM-5), resulting in the composition development in Figs. 5–6 and Table S3. Since the injected amount of MeOH (1.2  $\mu\text{mol}_C$  per pulse) is only a fraction of the total number of BAS (Table 1), the catalyst bed downstream of the active MTH zone, corresponding with an increasing amount of H-ZSM-5 (from 4.5 to 200 mg), can only affect processes like adsorption/desorption and secondary reactions in absence of MeOH. In particular, propylene and butylenes decrease while ethylene, butanes, propane, benzene, and toluene increase with increasing bed length, implying the simultaneous occurrence of (de-) alkylation, aromatization, and hydrogen transfer reactions specifically in the downstream zone of the bed. Ilias and Bhan proposed the ratio of ethylene to isobutane (mol C basis) as a qualitative descriptor to assess the relative contribution of the aromatic and olefinic cycle [16]. For the FASPA experiments with 1.2  $\mu\text{mol}$  MeOH (Table S3) these ratios amount to 0.79 and 0.93 for the 4.5 and 100 mg sample, respectively, indicating that care must be taken with applying this descriptor in full methanol conversion cases. The increasing ratio here does, however, point to further reactions downstream of the active reaction zone in the longer catalyst bed. More discussion about the impact of these secondary reactions on MTH product distribution and temporal responses is the topic of our following study.

Unlike aliphatics, BTX exhibits a two-peak response to the MeOH pulse over H-ZSM-5. The first response ‘R1’ appears nearly simultaneously with the aliphatics and the quick build-up of cyclic surface species (Fig. 3 and *in situ* DRIFT results in Fig. 4), implying that those aromatics are formed instantly from MeOH. With increasing catalyst amount this R1 response shows a chromatographic adsorption–desorption delay of BTX (cf. Fig. S11). The observed broad second BTX response (R2) also shows a delay, but much longer, and therefore cannot solely be an adsorption–desorption phenomenon of BTX species. Since in this response time frame no MeOH is present any more, they must originate from another source. In absence of MeOH the HCP will no longer be maintained, resulting in the breakdown of HCP species, comprising polyolefinic, substituted cyclopentenyl, and aromatic species [60,88], in line with reported spectroscopic observations [23,24]. Schulz attributed the activity loss in H-ZSM-5 at low temperatures (< 300 °C) to the formation of polyalkylated benzene species that cannot leave the MFI framework [17]. The reduced formation of propylene and butylenes with increasing catalyst amount indicates such alkylation by olefins. These blocking species may further undergo dealkylation (coined ‘reanimation’ by Schulz), releasing retarded BTX, which can

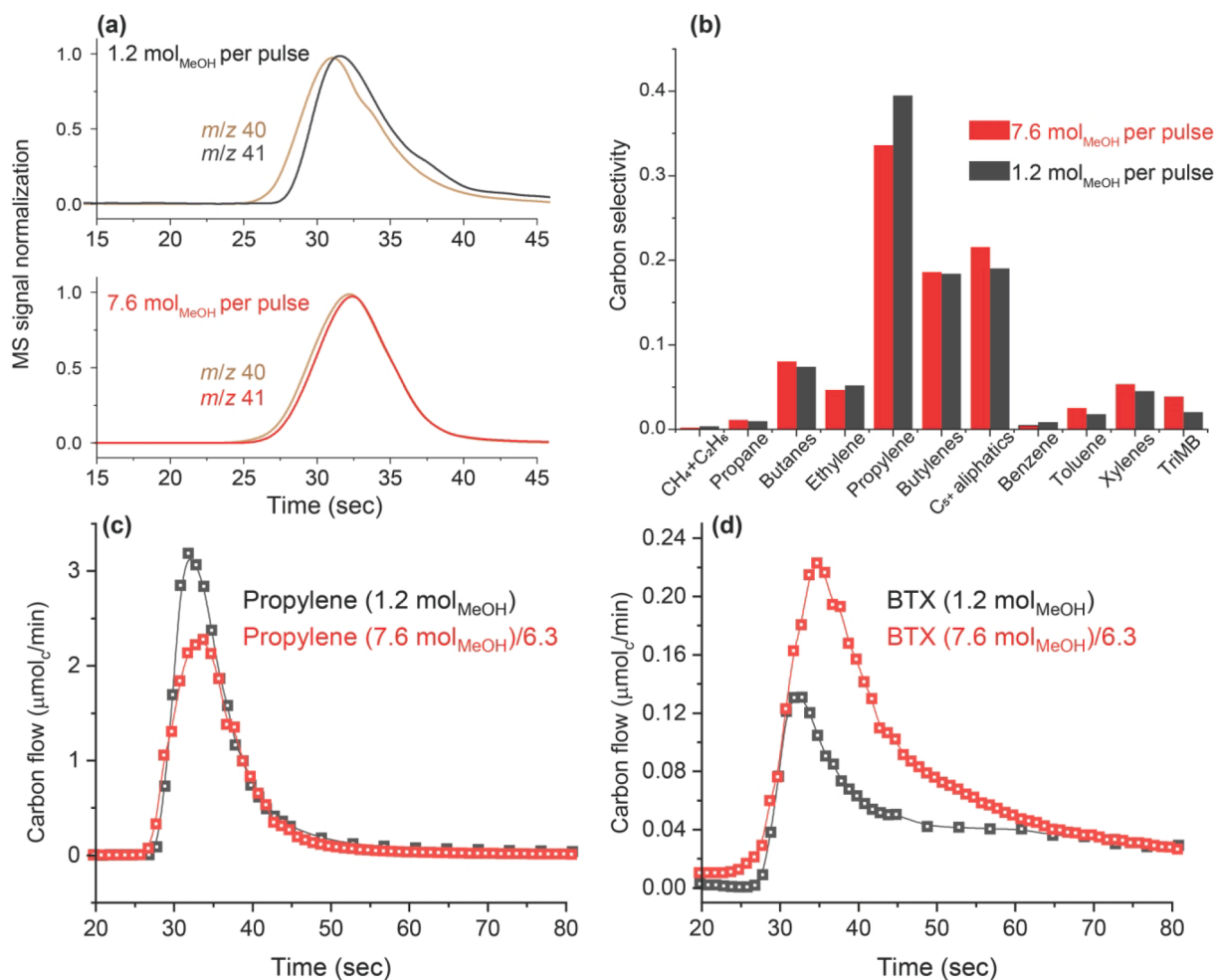


**Fig. 7.** (a) Normalized MS-pulse responses of  $m/z$  40 and 41 referring to Ar and aliphatic products; (b) total carbon selectivity of hydrocarbons; (c) propylene and (d) BTX temporal responses over H-ZSM-5 with different MeOH injection quantities in FASPA tests. Conditions:  $T = 400$  °C,  $m_{\text{cat}} = 4.5$  mg (H-ZSM-5, Si/Al 25, 150–212  $\mu\text{m}$ ),  $P_{\text{reactor}} = 1$  bar, MeOH pulse quantity 1.2 and 7.6  $\mu\text{mol}_{\text{C}}$  per pulse, carrier gas He = 20 mL<sub>NTP</sub>/min, pulse interval = 3.75 min. Note: carbon flows of propylene and BTX responses with 7.6  $\mu\text{mol}_{\text{C}}$  per pulse were divided by 6.3 for the direct comparison with those with 1.2  $\mu\text{mol}_{\text{C}}$  per pulse in the FASPA tests. More quantitative results and full scale of FASPA responses can be found in Table S4 and Fig. S6.

undergo similar alkylation/de-alkylation processes further down the bed [89]. The prolonged residence time in the bed allows the increasing formation of ethylene from substituted dimethyl benzenes (Table S3) as in the aromatic cycle [19,90]. This continuous olefin alkylation/de-alkylation of substituted benzenes can explain the broad retarded second maximum in the BTX appearance, showing the dynamics of this process with the appearance of a chromatographic reactor [91]. This is further evidenced when propylene is pulsed over 100 mg H-ZSM-5 at 400 °C, giving similar BTX responses as the 2<sup>nd</sup> BTX maxima observed in the MeOH pulse test (see Fig. S7). Clearly, propylene only also results in MTH reactions, contributing to aromatization products and appearance of the retarded 2<sup>nd</sup> BTX maxima via an HCP-like mechanism.

With a larger pulse size of 7.6  $\mu\text{mol}_{\text{C}}$  over the 4.5 mg H-ZSM-5, MeOH conversion is  $\sim 95$  % indicating the availability of MeOH along the whole catalyst bed. The time delay between Ar and the first hydrocarbon product (methane) in this case is much shorter than that obtained with a smaller pulse size of 1.2  $\mu\text{mol}_{\text{C}}$ . Müller *et al.* have identified two separate hydrogen transfer pathways, with one of them involving the participation of MeOH finally leading to a faster aromatic formation than the conventional olefin-mediated hydrogen transfer route [46]. In our FASPA results, the shortened time delay between Ar and hydrocarbons for a larger pulse size probably also indicates that the induction process for the HCP build-up or restoration is promoted by MeOH (with methane as a by-product in this process), further leading to a higher selectivity to

C<sub>5+</sub> aliphatics and aromatics once the HCP has been built up (Fig. 7).

The introduced FASPA technique is illustrated here for MTH over H-ZSM-5, but other conditions, catalysts and reactions can be analyzed by this method using quite standard research equipment. In principle, next to pulse-response also step-response experiments are amenable, yielding quantitative temporal composition information during the transient, relevant for mechanistic insight and design of multifunctional and non-steady state operated reactors [92–94].

## 5. Conclusions

The newly developed fast scanning-pulse analysis (FASPA) technique shows the potential to extract highly dynamic information and enables to distinguish highly coupled processes in the complex reaction network, for example, the MTH process. The zeolite catalysed MTH fixed-bed process often proceeds with full conversion of the MeOH fed, producing a mixture of alkanes, olefins and aromatics next to water over a gradually deactivating catalyst. Within this complex reaction network, many reactions including MeOH-mediated reactions and secondary reactions occur simultaneously and vary both in temporal and spatial dimension. This indicates a highly dynamic feature of the MTH process from the start-up induction period to the following steady-state process in the whole catalyst bed. Compared to the conventional steady-state operation for reaction mechanism studies, transient operation using

the robust FASPA approach discloses rich insights in the highly dynamic MTH process at realistic reaction conditions over freshly activated H-ZSM-5 catalyst. In particular:

- The second resolution of gas phase product responses upon the MeOH pulse reveal the fast consecutive reactions occurring in a narrow active MTH zone. All products appear nearly simultaneously after a short delay (a few seconds) upon MeOH injection, attributed to the HCP build-up induction period. This induction period can be sufficiently reduced by slightly elevating the reacting temperature by 30 °C or by increasing the MeOH quantity in each pulse. Methane is observed prior to other hydrocarbons, possibly related to the primary MeOH decomposition and disproportionation and the first C—C bond formation.
- Depending on the presence of MeOH or not, two consecutive pathways for aromatics formation were directly discerned and kinetically decoupled: a very fast primary product formation in the presence of MeOH, followed by a slower second formation of aromatics when MeOH is depleted. By combining *in situ* DRIFTS and FASPA experiments, the fast formation of BTX and aliphatics is primarily related to the build-up of hydrocarbon pool species including cyclopentenyl species and methylated benzenes. The secondary formation of BTX is then related to the rather slow decomposition/desorption of HCP species.
- Downstream of the active MTH zone where MeOH is fully converted, secondary reactions occur with increasing catalyst amount. Decomposed HCP species and olefins undergo aromatization and alkylation-dealkylation reaction, retarding the appearance of BTX, resulting in their broad secondary formation. The associated hydrogen transfer reactions result in an increased alkane formation, with (iso)butanes as the major component.

The core of the FASPA technique lies in the (un)synchronizing program that allows the fine control of online GC (or other instruments in other cases) sampling in the transient operations. As long as the prerequisites for *quasi* steady-state operating conditions are met, this (un)synchronization mechanism combining the pulse technique and online quantification tools can be easily extended to other reaction systems extracting transient kinetic information, which is of vital value for understanding the complex reaction mechanism and related catalyst design and improvement.

### Declaration of Competing Interest

The authors declare that they have no known competing financial interests or personal relationships that could have appeared to influence the work reported in this paper.

### Data availability

The data that support the findings of this study are openly available in Figshare at <https://doi.org/10.4121/21316656.v1>.

### Acknowledgements

The manuscript was written through contributions of all authors. All authors have given approval to the final version of the manuscript. We acknowledge BASF and the Advanced Research Center Chemical Building Blocks Consortium (ARC CBBC) for funding under project number 2016.007.TUD.

### Appendix A. Supplementary data

Supplementary data to this article can be found online at <https://doi.org/10.1016/j.cej.2022.139696>.

### References

- [1] R.A. Sheldon, Green and sustainable manufacture of chemicals from biomass: state of the art, *Green Chem.* 16 (3) (2014) 950–963.
- [2] Z. Sun, G. Bottari, A. Afanassenko, M.C. Stuart, P.J. Deuss, B. Fridrich, K. Barta, Complete lignocellulose conversion with integrated catalyst recycling yielding valuable aromatics and fuels, *Nat. Catal.* 1 (1) (2018) 82–92.
- [3] J. Wei, Q. Ge, R. Yao, Z. Wen, C. Fang, L. Guo, H. Xu, J. Sun, Directly converting CO<sub>2</sub> into a gasoline fuel, *Nat. Commun.* 8 (1) (2017) 1–9.
- [4] P.C. Bruijninx, B.M. Weckhuysen, Shale gas revolution: an opportunity for the production of biobased chemicals? *Angew. Chem. Int. Ed.* 52 (46) (2013) 11980–11987.
- [5] P. Tian, Y. Wei, M. Ye, Z. Liu, Methanol to olefins (MTO): from fundamentals to commercialization, *ACS Catal.* 5 (3) (2015) 1922–1938.
- [6] G. Iaquaniello, G. Centi, A. Salladini, E. Palo, Chapter 4 - Waste as a Source of Carbon for Methanol Production, in: *Methanol*, Elsevier, 2018, pp. 95–111.
- [7] C. Hobson, C. Márquez, Renewable Methanol Report, The Methanol Institute, Singapore, 2018.
- [8] M. Melikoglu, V. Singh, S.Y. Leu, C. Webb, C.S.K. Lin, et al., 9 - Biochemical Production of Bioalcohols, in: *Handbook of Biofuels Production (Second Edition)*, Woodhead Publishing, 2016, pp. 237–258.
- [9] F.J. Morales-Leal, J. Rivera De la Rosa, C.J. Lucio-Ortiz, D.A. De Haro Del, M. A. Río, W.T. Garza-Navarro, J.E. Herrera, Monometallic platinum and palladium-based catalysts in the competitive oxidation of methanol over the liquid-phase methanol-ethanol mixtures, *Chem. Eng. J.* 426 (2021), 131623.
- [10] W. Wang, A. Buchholz, M. Seiler, M. Hunger, Evidence for an initiation of the methanol-to-Olefin process by reactive Surface methoxy groups on acidic zeolite catalysts, *J. Am. Chem. Soc.* 125 (49) (2003) 15260–15267.
- [11] Y. Liu, S. Müller, D. Berger, J. Jelic, K. Reuter, M. Tonigold, M. Sanchez-Sanchez, J. A. Lercher, Formation mechanism of the first carbon-carbon bond and the first olefin in the methanol conversion into hydrocarbons, *Angew. Chem. Int. Ed.* 55 (19) (2016) 5723–5726.
- [12] A.D. Chowdhury, K. Houben, G.T. Whiting, M. Mokhtar, A.M. Asiri, S.A. Al-Thabaiti, S.N. Basahel, M. Baldus, B.M. Weckhuysen, Initial carbon-carbon bond formation during the early stages of the methanol-to-olefin process proven by zeolite-trapped acetate and methyl acetate, *Angew. Chem. Int. Ed.* 55 (51) (2016) 15840–15845.
- [13] T. Sun, W. Chen, S. Xu, A. Zheng, X. Wu, S. Zeng, N. Wang, X. Meng, Y. Wei, Z. Liu, The first carbon-carbon bond formation mechanism in methanol-to-hydrocarbons process over chabazite zeolite, *Chem* 7 (9) (2021) 2415–2428.
- [14] I. Yarulina, A.D. Chowdhury, F. Meirer, B.M. Weckhuysen, J. Gascon, Recent trends and fundamental insights in the methanol-to-hydrocarbons process, *Nat. Catal.* 1 (6) (2018) 398–411.
- [15] I.M. Dahl, S. Kolboe, On the reaction mechanism for propene formation in the MTO reaction over SAPO-34, *Catal. Lett.* 20 (3) (1993) 329–336.
- [16] S. Ilias, A. Bhan, Mechanism of the catalytic conversion of methanol to hydrocarbons, *ACS Catal.* 3 (1) (2013) 18–31.
- [17] H. Schulz, About the mechanism of methanol conversion on zeolites, *Catal. Lett.* 148 (5) (2018) 1263–1280.
- [18] I. Yarulina, F. Kapteijn, J. Gascon, The importance of heat effects in the methanol to hydrocarbons reaction over ZSM-5: on the role of mesoporosity on catalyst performance, *Catal. Sci. Technol.* 6 (14) (2016) 5320–5325.
- [19] S. Svelle, F. Joensen, J. Nerlov, U. Olsbye, K.-P. Lillerud, S. Kolboe, M. Bjørgen, Conversion of methanol into hydrocarbons over zeolite h-zsm-5: ethene formation is mechanistically separated from the formation of higher alkenes, *J. Am. Chem. Soc.* 128 (46) (2006) 14770–14771.
- [20] E.A. Redekop, A. Lazzarini, S. Bordiga, U. Olsbye, A Temporal Analysis of Products (TAP) Study of C<sub>2</sub>–C<sub>4</sub> Alkene Reactions with a well-defined pool of methylating species on ZSM-22 zeolite, *J. Catal.* 385 (2020) 300–312.
- [21] O. Dewaele, V.L. Geers, G.F. Froment, G.B. Marin, The conversion of methanol to olefins: a transient kinetic study, *Chem. Eng. Sci.* 54 (20) (1999) 4385–4395.
- [22] R.Y. Brogaard, R. Henry, Y. Schuurman, A.J. Medford, P.G. Moses, P. Beato, S. Svelle, J.K. Nørskov, U. Olsbye, Methanol-to-hydrocarbons conversion: the alkene methylation pathway, *J. Catal.* 314 (2014) 159–169.
- [23] J.F. Haw, J.B. Nicholas, W. Song, F. Deng, Z. Wang, T. Xu, C.S. Heneghan, Roles for cyclopentenyl cations in the synthesis of hydrocarbons from methanol on zeolite catalyst hzsm-5, *J. Am. Chem. Soc.* 122 (19) (2000) 4763–4775.
- [24] L. Zhang, S. Wang, Z. Qin, P. Wang, G. Wang, M. Dong, W. Fan, J. Wang, Probing into the building and evolution of primary hydrocarbon pool species in the process of methanol to olefins over H-ZSM-5 zeolite, *Mol. Catal.* 516 (2021), 111968.
- [25] C. Emeis, Determination of integrated molar extinction coefficients for infrared absorption bands of pyridine adsorbed on solid acid catalysts, *J. Catal.* 141 (2) (1993) 347–354.
- [26] C.J. Manning, R.A. Palmer, J.L. Chao, Step-scan Fourier-transform infrared spectrometer, *Rev. Sci. Instrum.* 62 (5) (1991) 1219–1229.
- [27] A. Liutkova, E. Uslamin, A. Parastayev, A. Bolshakov, B. Mezari, E.J.M. Hensen, N. Kosinov, A scanning pulse reaction technique for transient analysis of the methanol-to-hydrocarbons reaction, *Catal. Today* (2022), <https://doi.org/10.1016/j.cattod.2022.05.005>. In press.
- [28] D.D. Do, Adsorption and Diffusivity Measurement by a Chromatography Method, in: *Adsorption analysis: Equilibria and kinetics*, Imperial College Press, London, 1998, pp. 775–795.
- [29] D.M. Ruthven, Dynamics of Adsorption Columns: Single-Transition Systems, in: *Principles of Adsorption and Adsorption Processes*, John Wiley, New York, 1984, pp. 220–273.

- [30] J.A. Moulijn, Stimulus/response experimenten in gepakte bedden, PhD Thesis, University of Amsterdam, Amsterdam, 1974.
- [31] E. Kubin, Beitrag zur Theorie der Chromatographie II. Einfluss der Diffusion ausserhalb und der Adsorption innerhalb des Sorbens-korns, Collect. Czech. Chem. Commun. 30 (1965) 2900–2907.
- [32] E. Kubin, Beitrag zur Theorie der Chromatographie, Collect. Czech. Chem. Commun. 30 (4) (1965) 1104–1118.
- [33] E. Kučera, Contribution to the theory of chromatography: Linear non-equilibrium elution chromatography, J. Chromatogr. A 19 (1965) 237–248.
- [34] O. Grubner, M. Ralek, A. Zikánová, Calculation of the mass-transfer coefficients by means of a more exact theory of gas-solid chromatography. I. Comparison of columns charged with glass spheres and materials of high internal porosity, Collect. Czech. Chem. Commun. 31 (1966) 852–862.
- [35] O. Grubner, A. Zikánová, M. Rálek, Statistical moments theory of gas-solid chromatography: Diffusion controlled kinetics, J. Chromatogr. A 28 (1967) 209–218.
- [36] P. Schneider, J.M. Smith, Adsorption rate constants from chromatography, AIChE J. 14 (5) (1968) 762–771.
- [37] S. Qamar, J.N. Abbasi, S. Javeed, M. Shah, F.U. Khan, A. Seidel-Morgenstern, Analytical solutions and moment analysis of chromatographic models for rectangular pulse injections, J. Chromatogr. A 1315 (2013) 92–106.
- [38] K.K. Chan, M.B. Bolger, K.S. Pang, Statistical moment theory in chemical kinetics, Anal. Chem. 57 (11) (1985) 2145–2151.
- [39] J.T. Gleaves, J.R. Ebner, T.C. Kuechler, Temporal Analysis of Products (TAP)—A Unique Catalyst Evaluation System with Submillisecond Time Resolution, Catal. Rev. 30 (1) (1988) 49–116.
- [40] G.S. Yablonskii, S.O. Shekhtman, S. Chen, J.T. Gleaves, Moment-Based Analysis of Transient Response Catalytic Studies (TAP Experiment), Ind. Eng. Chem. Res. 37 (6) (1998) 2193–2202.
- [41] S.O. Shekhtman, G.S. Yablonsky, J.T. Gleaves, R. Fushimi, “State defining” experiment in chemical kinetics—primary characterization of catalyst activity in a TAP experiment, Chem. Eng. Sci. 58 (21) (2003) 4843–4859.
- [42] J.A. Moulijn, J.F.M. Kolk, H.F.M. Reijnders, Incorporation of Surface Migration in the Theory of Gas-Solid Chromatography, Ind. Eng. Chem. Fundam. 16 (2) (1977) 301–303.
- [43] W. Wang, M. Hunger, Reactivity of Surface Alkoxy Species on Acidic Zeolite Catalysts, Acc. Chem. Res. 41 (8) (2008) 895–904.
- [44] Z. Chen, W. Song, Y. Hou, H. Wang, C. Zhang, J. Wang, Y. Yang, W. Qian, Temperature-dependent secondary conversion of primary products from methanol aromatization in a two-stage fluidized bed, Fuel 267 (2020), 117204.
- [45] H. Krannila, W.O. Haag, B.C. Gates, Monomolecular and bimolecular mechanisms of paraffin cracking: n-butane cracking catalyzed by HZSM-5, J. Catal. 135 (1) (1992) 115–124.
- [46] S. Müller, Y. Liu, F.M. Kirchberger, M. Tonigold, M. Sanchez-Sanchez, J.A. Lercher, Hydrogen Transfer Pathways during Zeolite Catalyzed Methanol Conversion to Hydrocarbons, J. Am. Chem. Soc. 138 (49) (2016) 15994–16003.
- [47] I. Yarullina, K. De Wispelaere, S. Baillieu, J. Goetze, M. Radersma, E. Abou-Hamad, I. Volmer, M. Goesten, B. Mezari, E.J.M. Hensen, J.S. Martínez-Espín, M. Morten, S. Mitchell, J. Perez-Ramirez, U. Olsbye, B.M. Weckhuysen, V. Van Speybroeck, F. Kapteijn, J. Gascon, Structure–performance descriptors and the role of Lewis acidity in the methanol-to-propylene process, Nat. Chem. 10 (8) (2018) 804–812.
- [48] W.O. Haag, R.M. Lago, P.G. Rodewald, Aromatics, light olefins and gasoline from methanol: Mechanistic pathways with ZSM-5 zeolite catalyst, J. Mol. Catal. 17 (2–3) (1982) 161–169.
- [49] E.D. Hernandez, F.C. Jentoft, Spectroscopic Signatures Reveal Cyclopentenyl Cation Contributions in Methanol-to-Olefins Catalysis, ACS Catal. 10 (10) (2020) 5764–5782.
- [50] A.V. Demidov, A.A. Davydov, Spectroscopic evidence for the formation of carbenium ions on H-ZSM-5 zeolites, Mater. Chem. Phys. 39 (1) (1994) 13–20.
- [51] I. Kiricsi, H. Förster, G. Tasi, J.B. Nagy, Generation, Characterization, and Transformations of Unsaturated Carbenium Ions in Zeolites, Chem. Rev. 99 (8) (1999) 2085–2114.
- [52] I. Kiricsi, H. Förster, Chemisorption of propene on HZSM-5 by ultraviolet and infrared spectroscopy, J. Chem. Soc., Faraday Trans. 1 F 84 (2) (1988) 491–499.
- [53] C. Pazé, B. Sazak, A. Zecchina, J. Dwyer, FTIR and UV–Vis Spectroscopic Study of Interaction of 1-Butene on H–Ferrierite Zeolite, J. Phys. Chem. B 103 (45) (1999) 9978–9986.
- [54] H. Förster, I. Kiricsi, J. Seebode, UV-Vis and IR Spectroscopic Investigations on the Generation of Alkenyl Carbocations from Propene in Zeolites of Different Acidity, in: Stud. Surf. Sci. Catal., Elsevier, Amsterdam, 1988, pp. 435–442.
- [55] J. Valcillos, E. Epelde, J. Albo, A.T. Aguayo, J. Bilbao, P. Castaño, Slowing down the deactivation of H-ZSM-5 zeolite catalyst in the methanol-to-olefin (MTO) reaction by P or Zn modifications, Catal. Today 348 (2020) 243–256.
- [56] C.W. Bauschlicher, E. Peeters, L.J. Allamandola, The infrared spectra of very large irregular polycyclic aromatic hydrocarbons (PAHs): observational probes of astronomical PAH geometry, size, and charge, Astrophys. J. 697 (1) (2009) 311–327.
- [57] F.C. Meunier, L. Domokos, K. Seshan, J.A. Lercher, In Situ IR Study of the Nature and Mobility of Sorbed Species on H-FER during But-1-ene Isomerization, J. Catal. 211 (2) (2002) 366–378.
- [58] A.G. Stepanov, V.N. Sidelnikov, K.I. Zamaraev, In Situ <sup>13</sup>C Solid-State NMR and Ex Situ GC–MS Analysis of the Products of tert-Butyl Alcohol Dehydration on H-ZSM-5 Zeolite Catalyst, Chem. Eur. J. 2 (2) (1996) 157–167.
- [59] J.D. Mosley, J.W. Young, J. Agarwal, H.F. Schaefer III, P.v.R. Schleyer, M. A. Duncan, Structural Isomerization of the Gas-Phase 2-Norbornyl Cation Revealed with Infrared Spectroscopy and Computational Chemistry, Angew. Chem. Int. Ed. 53 (23) (2014) 5888–5891.
- [60] W. Zhang, M. Zhang, S. Xu, S. Gao, Y. Wei, Z. Liu, Methylcyclopentenyl Cations Linking Initial Stage and Highly Efficient Stage in Methanol-to-Hydrocarbon Process, ACS Catal. 10 (8) (2020) 4510–4516.
- [61] C. Wang, X. Sun, J. Xu, G. Qi, W. Wang, X. Zhao, W. Li, Q. Wang, F. Deng, Impact of temporal and spatial distribution of hydrocarbon pool on methanol conversion over H-ZSM-5, J. Catal. 354 (2017) 138–151.
- [62] X. Wu, S. Xu, W. Zhang, J. Huang, J. Li, B. Yu, Y. Wei, Z. Liu, Direct Mechanism of the First Carbon-Carbon Bond Formation in the Methanol-to-Hydrocarbons Process, Angew. Chem. Int. Ed. 56 (31) (2017) 9039–9043.
- [63] L. Yang, T. Yan, C. Wang, W. Dai, G. Wu, M. Hunger, W. Fan, Z. Xie, N. Guan, L. Li, Role of Acetaldehyde in the Roadmap from Initial Carbon-Carbon Bonds to Hydrocarbons during Methanol Conversion, ACS Catal. 9 (7) (2019) 6491–6501.
- [64] L. Yang, C. Wang, W. Dai, G. Wu, N. Guan, L. Li, Progressive steps and catalytic cycles in methanol-to-hydrocarbons reaction over acidic zeolites, Fundam. Res. 2 (2) (2022) 184–192.
- [65] Y. Liu, F.M. Kirchberger, S. Müller, M. Eder, M. Tonigold, M. Sanchez-Sanchez, J. A. Lercher, Critical role of formaldehyde during methanol conversion to hydrocarbons, Nat. Commun. 10 (1) (2019) 1462.
- [66] A. Comas-Vives, M. Valla, C. Copéret, P. Sautet, Cooperativity between Al Sites Promotes Hydrogen Transfer and Carbon-Carbon Bond Formation upon Dimethyl Ether Activation on Alumina, ACS Cent. Sci. 1 (6) (2015) 313–319.
- [67] T. Yokoi, H. Mochizuki, S. Namba, J.N. Kondo, T. Tatsumi, Control of the Al Distribution in the Framework of ZSM-5 Zeolite and Its Evaluation by Solid-State NMR Technique and Catalytic Properties, J. Phys. Chem. C 119 (27) (2015) 15303–15315.
- [68] T.R. Forester, R.F. Howe, In situ FTIR studies of methanol and dimethyl ether in ZSM-5, J. Am. Chem. Soc. 109 (17) (1987) 5076–5082.
- [69] K. Kubo, H. Iida, S. Namba, A. Igarashi, Selective Formation of Light Olefins by Catalytic Cracking of Naphtha Components over ZSM-5 Zeolite Catalysts, J. Japan Pet. Inst. 61 (1) (2018) 10–19.
- [70] R. Khare, Z. Liu, Y. Han, A. Bhan, A mechanistic basis for the effect of aluminum content on ethene selectivity in methanol-to-hydrocarbons conversion on HZSM-5, J. Catal. 348 (2017) 300–305.
- [71] R. Khare, D. Millar, A. Bhan, A mechanistic basis for the effects of crystallite size on light olefin selectivity in methanol-to-hydrocarbons conversion on MFI, J. Catal. 321 (2015) 23–31.
- [72] R. Khare, S.S. Arora, A. Bhan, Implications of Cofeeding Acetaldehyde on Ethene Selectivity in Methanol-to-Hydrocarbons Conversion on MFI and Its Mechanistic Interpretation, ACS Catal. 6 (4) (2016) 2314–2331.
- [73] K. Morgan, J. Toutou, J.-S. Choi, C. Coney, C. Hardacre, J.A. Pihl, C.E. Stere, M.-Y. Kim, C. Stewart, A. Goguet, W.P. Partridge, Evolution and Enabling Capabilities of Spatially Resolved Techniques for the Characterization of Heterogeneously Catalyzed Reactions, ACS Catal. 6 (2) (2016) 1356–1381.
- [74] K. Morgan, N. Maguire, R. Fushimi, J.T. Gleaves, A. Goguet, M.P. Harold, E. V. Kondratenko, U. Menon, Y. Schuurman, G.S. Yablonsky, Forty years of temporal analysis of products, Catal. Sci. Technol. 7 (12) (2017) 2416–2439.
- [75] S.K. Gangwal, R.R. Hudgins, P.L. Silveston, Reliability and limitations of pulse chromatography in evaluating properties of flow systems: 1. modelling and experimental considerations, Can. J. Chem. Eng. 57 (5) (1979) 609–620.
- [76] V. Fierro, Y. Schuurman, Simultaneous determination of intrinsic adsorption and diffusion of n-butane in activated carbons by using the TAP reactor, in: Stud. Surf. Sci. Catal., Elsevier, Amsterdam, 2007, pp. 241–247.
- [77] E.B. Boz, A. Taşdemir, E. Biçer, A. Yürüm, S. Alkan Gürsel, Emergent hierarchical porosity by ZIF-8/GO nanocomposite increases oxygen electroreduction activity of Pt nanoparticles, Int. J. Hydrogen Energy 46 (65) (2021) 32858–32870.
- [78] H. Stach, U. Lohse, H. Thamm, W. Schirmer, Adsorption equilibria of hydrocarbons on highly dealuminated zeolites, Zeolites 6 (2) (1986) 74–90.
- [79] C.G. Pope, Sorption of benzene, toluene, and para-xylene on ZSM-5, J. Phys. Chem. 88 (25) (1984) 6312–6313.
- [80] C.G. Pope, Sorption of benzene, toluene and p-xylene on silicalite and H-ZSM-5, J. Phys. Chem. 90 (5) (1986) 835–837.
- [81] C.G. Pope, Adsorption of methanol and related molecules on zeolite H-ZSM-5 and silicalite, J. Chem. Soc., Faraday Trans. 89 (7) (1993) 1139–1141.
- [82] C.K. Lee, A.S.T. Chiang, Adsorption of aromatic compounds in large MFI zeolite crystals, J. Chem. Soc., Faraday Trans. 92 (18) (1996) 3445–3451.
- [83] R.R. Mukti, A. Jentys, J.A. Lercher, Orientation of alkyl-substituted aromatic molecules during sorption in the pores of WZSM-5 zeolites, J. Phys. Chem. C 111 (10) (2007) 3973–3980.
- [84] A. Jentys, R.R. Mukti, H. Tanaka, J.A. Lercher, Energetic and entropic contributions controlling the sorption of benzene in zeolites, Microporous Mesoporous Mater. 90 (1–3) (2006) 284–292.
- [85] J.M. Kanervo, S. Kouva, K.J. Kanervo, R. Kolvenbach, A. Jentys, J.A. Lercher, Prerequisites for kinetic modeling of TPD data of porous catalysts—Exemplified by toluene/H-ZSM-5 system, Chem. Eng. Sci. 137 (2015) 807–815.
- [86] T. Omojola, Site-specific scaling relations observed during methanol-to-olefin conversion over ZSM-5 catalysts, Chem. Eng. Sci. 251 (2022), 117424.
- [87] R. Khare, A. Bhan, Mechanistic studies of methanol-to-hydrocarbons conversion on diffusion-free MFI samples, J. Catal. 329 (2015) 218–228.
- [88] S. Lin, Y. Zhi, W. Chen, H. Li, W. Zhang, C. Lou, X. Wu, S. Zeng, S. Xu, J. Xiao, A. Zheng, Y. Wei, Z. Liu, Molecular Routes of Dynamic Autocatalysis for Methanol-to-Hydrocarbons Reaction, J. Am. Chem. Soc. 143 (31) (2021) 12038–12052.
- [89] S. Al-Khattaf, S.A. Ali, A.M. Aitani, N. Žilková, D. Kubička, J. Čejka, Recent Advances in Reactions of Alkylbenzenes Over Novel Zeolites: The Effects of Zeolite Structure and Morphology, Catal. Rev. 56 (4) (2014) 333–402.

- [90] C. Wang, X. Yi, J. Xu, G. Qi, P. Gao, W. Wang, Y. Chu, Q. Wang, N. Feng, X. Liu, A. Zheng, F. Deng, Experimental Evidence on the Formation of Ethene through Carbocations in Methanol Conversion over H-ZSM-5 Zeolite, *Chem. Eur. J.* 21 (34) (2015) 12061–12068.
- [91] V. Russo, R. Tesser, C. Rossano, R. Vitiello, R. Turco, T. Salmi, M. Di Serio, Chromatographic reactor modelling, *Chem. Eng. J.* 377 (2019), 119692.
- [92] R. Krishna, Reactive separations: more ways to skin a cat, *Chem. Eng. Sci.* 57 (9) (2002) 1491–1504.
- [93] A. Renken, Transient processes in modeling heterogeneous catalytic kinetics, *Chem. Ing. Tech.* 62 (9) (1990) 724–756.
- [94] K.F. Kalz, R. Kraehnert, M. Dvoyashkin, R. Dittmeyer, R. Gläser, U. Krewer, K. Reuter, J.-D. Grunwaldt, Future Challenges in Heterogeneous Catalysis: Understanding Catalysts under Dynamic Reaction Conditions, *ChemCatChem* 9 (1) (2017) 17–29.